ACS APPLIED MATERIALS & INTERFACES

www.acsami.org

Research Article

Guanidinium-Perfunctionalized Polyhedral Oligomeric Silsesquioxanes as Highly Potent Antimicrobials against Planktonic Microbes, Biofilms, and Coronavirus

Ning Li,* He-Kuan Luo, Adrielle Xianwen Chen, Jeremy Pang Kern Tan, Chuan Yang, Melgious Jin Yan Ang, Huaqiang Zeng,* and Yi Yan Yang*

Cite This: *ACS Appl. Mater. Interfaces* 2023, 15, 354−363

Read Online

ACCESS | Metrics & More | Article Recommendations | Supporting Information

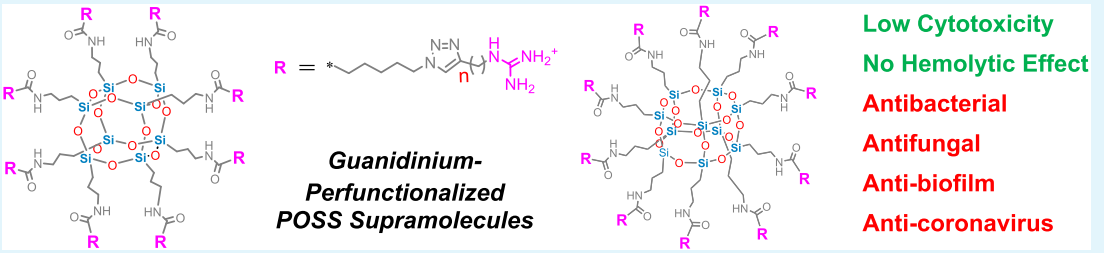

ABSTRACT: Supramolecules have been drawing increasing attention recently in addressing healthcare challenges caused by infectious pathogens. We herein report a novel class of guanidinium-perfunctionalized polyhedral oligomeric silsesquioxane (Gua-POSS) supramolecules with highly potent antimicrobial activities. The modular structure of Gua-POSS **T*m*-C*n*** consists of an inorganic T10 or T8 core (m = 10 or 8), flexible linear linkers of varying lengths (n = 1 or 3), and peripherally aligned cationic guanidinium groups as the membrane-binding units. Such Gua-POSS supramolecules with spherically arrayed guanidinium cations display high antimicrobial potency against Gram-positive (*Staphylococcus aureus*) and Gram-negative (*Escherichia coli*) bacteria, as well as fungus (*Candida albicans*), with the best showing excellently low minimal inhibitory concentrations (MICs) of 1.7−6.8 μM in media, yet with negligible hemolytic activity and low *in vitro* cytotoxicity to mammalian cells. More significantly, they can inhibit biofilm formation at around their MICs and near-completely break down preestablished difficult-to-break biofilms at 250 μg mL^{-1} (~50 μM). Their strong antiviral efficacy was also experimentally demonstrated against the enveloped murine hepatitis coronavirus as a surrogate of the SARS-CoV species. Overall, this study provides a new design approach to novel classes of sphere-shaped organic−inorganic hybrid supramolecular materials, especially for potent antimicrobial, anti-biofilm, and antiviral applications.

KEYWORDS: *antimicrobial, antiviral agents, biofilm, guanidinium, supramolecular chemistry*

1. INTRODUCTION

A wave of severe infectious disease outbreaks, mostly of viral origin (e.g., 2003 SARS, 2012 MERS, and the current Covid-19), has been witnessed in the first 20 years of the 21st century and tremendously impacted lives, economies, and healthcare systems all around the world.[1] Equally worrying, if not more, are bacterial infections reemerged as critical health threats to humans, ascribed to the misuse and overuse of antibiotics in the past few decades.[2,3] In particular, biofilm-related complications are widely considered as one of the major medical challenges, accounting for over 60% of chronic infections and countless casualties worldwide.[4−6] Protected by the self-secreted extracellular matrix (ECM),[7] bacteria enclosed in biofilms can be over 10^3 times more resistant to antibiotics than their planktonic counterparts, posing a significant challenge in inhibiting biofilm formation and more importantly in breaking down the preformed tenacious biofilms on medical apparatus, implants, nosocomial facilities, etc.[8]

Despite the pressing needs, most antibiotics, either existing or those under development, are not able to combat biofilms, possibly because of the ECM shielding barrier that prevents antibiotics from penetrating into the matrix.[9] Antimicrobial peptides, though effective in biofilm dispersion, are costly and subject to enzymatic degradation under *in vivo* conditions.[10] Cationic amphiphilic polymers represent another novel class of potent antimicrobial materials that have garnered intense research interests recently.[11−16] For such polymers, the two

Received: September 13, 2022
Accepted: December 7, 2022
Published: December 19, 2022

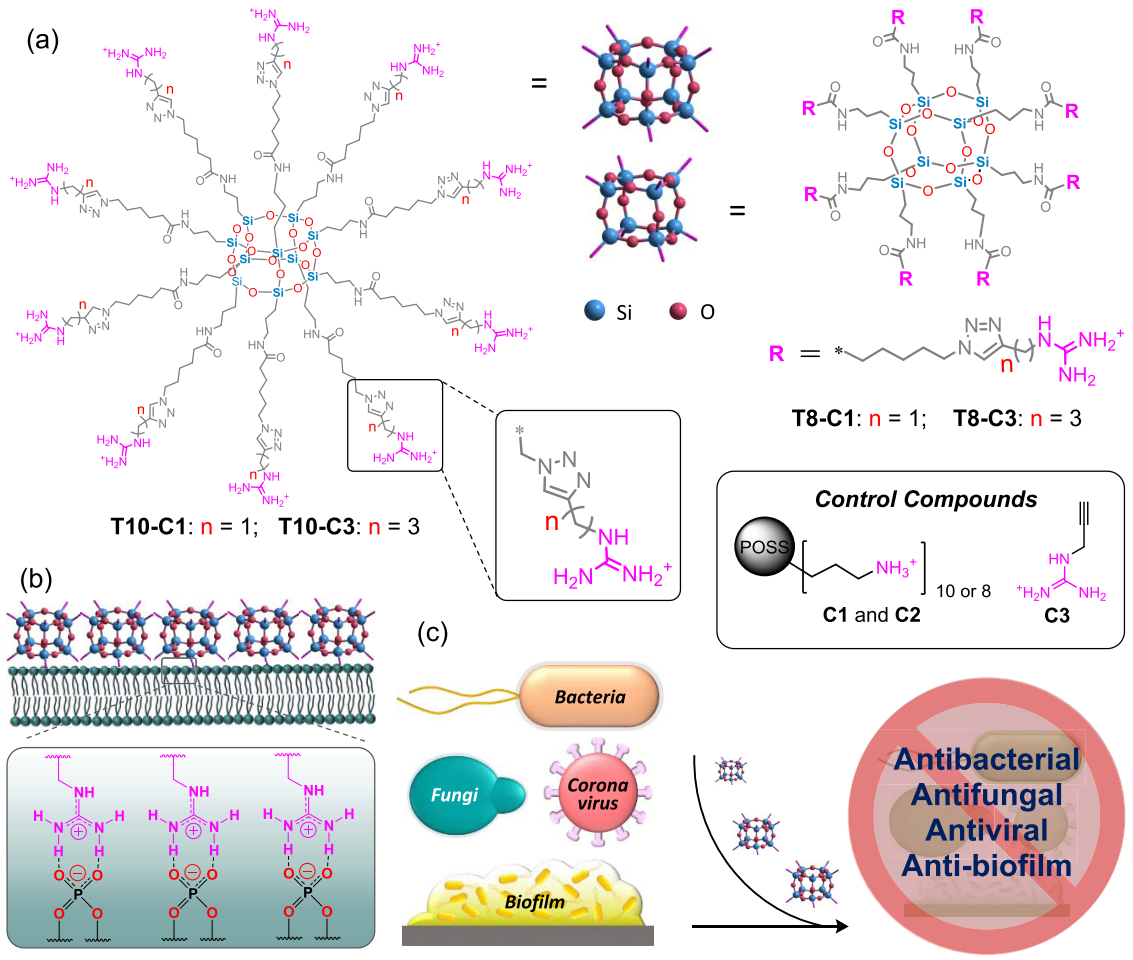

Figure 1. (a) Structure of Gua-POSS supramolecular designs and control compounds; counter ions (*i.e.*, trifluoroacetate for Gua-POSS and **C3**, triflate for **C1** and **C2**) are not shown. (b) Possible binding mode between the cationic guanidiniums and anionic phosphates on the lipid membrane via electrostatic interactions and hydrogen bonding; adapted from ref 26, Copyright 2014, American Chemical Society. (c) Illustration of bacteria and fungi killing, coronavirus inactivation, and biofilm disruption by Gua-POSS supramolecules. The drawings of Gua-POSS, bacteria, fungi, and coronavirus are not to scale.

basic indexes, namely, molecular weight and polydispersity, can significantly influence their interactions with bacteria and mammalian cells.[17−20] Nonetheless, it is still a challenging task to correlate each species of different molecular weights in the polydispersed mixture with their respective antimicrobial performance, thereby hindering the establishment of unambiguous structure−activity relations (SAR). Further development of safe and effective antimicrobials and antivirals to combat wide-ranging forms of infectious pathogens, e.g., planktonic bacteria, fungi, biofilms, and viruses, is therefore an urgent task to safeguard public health and meanwhile better prepare us for "*Disease X*" in the next outbreak.

Large columnar molecules carrying multiple active moieties have recently shown great promise as antimicrobial and anti-biofilm agents by virtue of their discrete molecular nature and preorganized functional groups.[21−25] In 2016, Cohen and co-workers reported a novel class of supramolecular pillar[5]-arenes decorated with phosphonium[21] or ammonium[22] groups. Although capable of inhibiting biofilm formation, they did not affect bacterial growth or disrupt preestablished biofilms. Haag and co-workers later designed a nanoaggregate self-assembly of zwitterionic pillar[5]arene macrocycles.[23] Such nanoaggregates of weak cationic nature displayed good destructive effects against bacteria both in the planktonic state and enclosed in the biofilm. Very recently, the pillar[5]arene scaffold was further functionalized with cationic guanidinium groups by Wang and co-workers,[24] which exhibited potent antibacterial activity against *Escherichia coli* and *Staphylococcus aureus*, and was also able to disrupt preformed *E. coli* biofilms. These studies have served to mark the potential of multiarmed molecules for antimicrobial applications, but the influence of different molecular core structures and three-dimensional (3D) spatial arrangement of peripheral functional ligands remain underexplored, as the prior examples were all built upon the same macrocyclic pillar[5]arene scaffold with a column-shaped configuration.[21−25]

Herein, we report a novel class of structurally well-defined high-purity polyhedral oligomeric silsesquioxane (POSS) supramolecules in spherical shape that are perfunctionalized with cationic guanidinium groups (Gua-POSS, Figure 1). Selected sphere-shaped Gua-POSS designs with T10 core demonstrate high potency against planktonic bacteria and fungi (MICs = 7.8−31.3 μg mL^{-1} in MHB media, equivalent to 1.7−6.8 μM), outperforming some column-shaped antibacterial designs,[23,24] yet with negligible hemolytic activity (HC_{50} > 2000 μg mL^{-1} on rat red blood cells) and low *in vitro* cytotoxicity (IC_{50} = 337.6−426.6 μg mL^{-1} to mouse fibroblast). More remarkably, they also display excellent

https://doi.org/10.1021/acsami.2c16493
ACS Appl. Mater. Interfaces 2023, 15, 354−363

performance to inhibit biofilm formation at around their respective MICs, and to near-completely disrupt and remove preestablished biofilms of different maturity stages at 250 μg mL^{-1} (~50 μM) in media. Additionally, they can also effectively inactivate the enveloped murine hepatitis coronavirus as a safe surrogate of the notorious SARS-CoV species, thereby providing a promising avenue against various types of infectious pathogens.

2. RESULTS AND DISCUSSION

2.1. Gua-POSS Supramolecular Designs. The Gua-POSS structure is modularly tunable, consisting of a T10 or T8 core, flexible linear linkers of varying lengths, and ten or eight peripheral cationic guanidinium groups as the target-binding moieties (Figure 1a). In the literature, guanidinium and its derivatives have been of extensive research interests for decades, ascribed to their antimicrobial activity and membrane-binding/penetrating capability.[27−31] In the Gua-POSS core of pentagonal prism (T10) or cubic (T8) shape, each tetrahedral Si center bonds to three μ_2-oxo bridges in the inorganic core and one side arm pointing outward, spatially preorganizing the terminal-appended guanidinium to form a spherical shape for potential antimicrobial actions. The linear linkers consist of three segments of alkyl chains, including C_3H_6, C_5H_{10}, and C_nH_{2n} (n = 1, 3) in length, respectively, interconnected by amide and 1,2,3-triazole linkages. These alkyl chains were crucial to render structural flexibility and also to enhance lipophilicity of the Gua-POSS supramolecules, both being essential factors influencing their interactions with the microbial lipid bilayer membrane.[32−35]

Four Gua-POSS designs were combinatorially synthesized with different cores and side chain lengths, namely, **T10-C1**, **T10-C3**, **T8-C1**, and **T8-C3** (Figure 1a). Their estimated physical dimensions range 5−8 nm at the most extended state, which are much smaller than typical microbial cells (0.5−5 μm) and viruses (20−200 nm), ensuring their good contact upon being mixed in solution to facilitate electrostatic and hydrophobic interactions with the pathogens. Additionally, Gua-POSS molecules with shorter linkers (*i.e.*, **T10-C1** and **T8-C1**) were isolated as yellow solids, whereas those with longer ones are orange-colored highly viscous liquids. They are well soluble in water and dimethyl sulfoxide, but only moderately soluble in methanol. POSS cages, mostly with T8 core, have been popularly used as a structural component for novel materials design, by virtue of their well-defined structures and hybrid properties from both the inorganic siloxane cage and organic peripheral groups.[36−38] Nonetheless, the active components in previous POSS-derived materials were usually not clearly described, being either a mixture of similar species[36] or dendrimer-like molecules with precise structures unknown.[38] Perfunctionalization of POSS into well-defined single molecular species is indeed synthetically challenging, and to our best knowledge, there has been no guanidinium-functionalized POSS examples reported in the literature. All Gua-POSS designs in the present study were isolated as single molecular species, thoroughly characterized by solution NMR spectroscopy (^{1}H, ^{13}C, and ^{29}Si) and electrospray ionization mass spectrometry (ESI-MS) to confirm their molecular structures, chemical purities, and structural stabilities in solution (see the Supporting Information for details). In light of the preorganized cationic guanidinium groups and hydrophobic flexible alkyl linkers, we envisioned that such appropriately structured Gua-POSS supramolecules of spherical shape would be able to act against various pathogenic microbes and viruses.

2.2. Antimicrobial Activity against Planktonic Microbes. Antimicrobial activities of Gua-POSS were investigated against a range of opportunistic human pathogens including Gram-negative bacterium *E. coli* (ATCC 25922), Gram-positive bacterium *S. aureus* (ATCC 6538), and fungus *C. albicans* (ATCC 10231). Their minimum inhibitory concentrations (MICs) and minimum bactericidal/fungicidal concentrations (MBCs/MFCs) were determined using the 2-fold microdilution approach in Mueller−Hinton Broth (MHB).[39] As shown in Table 1, they all display high potency against the three target species, with MICs in the 7.8−62.5 μg mL^{-1} range and MBCs/MFCs that are 1−3 times higher than respective MICs. Such values are in a similar range to those of some best-performing cationic polymers developed in our lab[11,39] and superior to those of the abovementioned pillar[5]arene-based columnar molecules, although the performance of which was characterized in M9 media[24] or simply PBS.[23] In addition, Gua-POSS's inhibitory effect was found to be stronger against bacteria *E. coli* and *S. aureus*, as compared to fungus *C. albicans*. We note that the T10-containing Gua-POSS outperformed their T8-containing counterparts in antimicrobial activities, although the difference was rather insignificant. A similar phenomenon was also observed in other *in vitro* biological tests (e.g., hemolytic activity, cytotoxicity, anti-biofilm activity; see details in later discussion). This could be due to the different number of guanidinium groups and their spatial arrangement in the molecular design, which will be the subject of further investigations. The effect of linker length alternation (n = 1 or 3) on the overall antimicrobial activity, however, was not seen, possibly because of the strong electrostatic interactions between Gua-POSS and microbial cells that mask the marginal hydrophobicity increase by the alkyl linker length extension.

Table 1. Summary of Minimum Inhibitory Concentrations (MICs) and Minimum Bactericidal/Fungicidal Concentrations (MBCs/MFCs) of Gua-POSS in Mueller−Hinton Broth against *E. coli*, *S. aureus*, and *C. albicans* in Units of μg mL^{-1}

	E. coli		*S. aureus*		*C. albicans*	
	MIC	MBC	MIC	MBC	MIC	MFC
T10-C1	15.6	15.6	7.8	31.3	31.3	62.5
T10-C3	15.6	15.6	15.6	31.3	31.3	62.5
T8-C1	15.6	31.3	15.6	62.5	62.5	125
T8-C3	15.6	31.3	15.6	62.5	62.5	125

2.3. Antimicrobial Mechanisms. Similar to cationic polymers and others,[11,39−41] we hypothesized that the antimicrobial activity of these positively charged Gua-POSS supramolecules is achieved via nonspecific electrostatic interactions with the negatively charged microbial cells, leading to membrane disruption followed by lysis and cell death, and we confirmed this hypothesis with the following experiments.

All three microbial cells (*i.e.*, *E. coli*, *S. aureus*, *C. albicans*) were found to be highly negatively charged in deionized water with ζ potentials of −21 to −51 mV, whereas upon freshly mixing with 250 μg mL^{-1} Gua-POSS, positive or near-zero ζ potentials (−2 to +36 mV) were recorded (Figure S1). This may serve as an experimental evidence for the electrostatic interactions between Gua-POSS and the microbes.[38,42]

https://doi.org/10.1021/acsami.2c16493
ACS Appl. Mater. Interfaces 2023, 15, 354−363

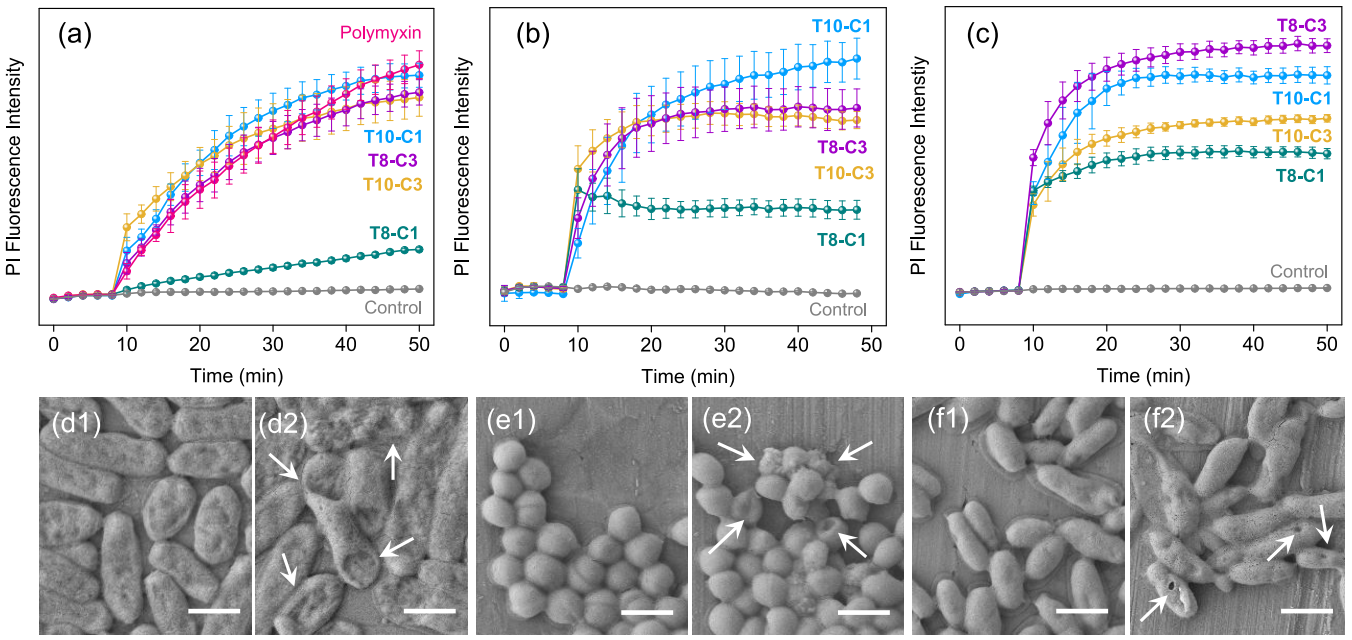

Figure 2. Time-dependent profile of PI fluorescence intensity to monitor microbial membrane permeability upon treatment with Gua-POSS at 125 μg mL^{-1}: (a) *E. coli*, (b) *S. aureus*, and (c) *C. albicans*. Three replicates were measured for each sample, and the results were expressed as the average value with standard deviation shown as the error bar. Representative FESEM images of (d) *E. coli*, (e) *S. aureus*, and (f) *C. albicans* treated with **T8-C1** at 250 μg mL^{-1}. Panels (d1), (e1), and (f1) are untreated bacterial/fungal cells as the negative control, while panels (d2), (e2), and (f2) are the bacterial/fungal cells after treatment. Scale bar is 1 μm. The arrows indicate exemplary sites of membrane disruption. Other Gua-POSS all demonstrate disrupted membranes under FESEM (see Figure S5).

However, it is worth noting that the positive charge is not the sole factor in determining the antimicrobial performance, evidenced by the observation that identical T10 or T8 cores functionalized with cationic ammonium groups (**C1** and **C2**, Figure 1a) were noneffective in inhibiting the microbial growth, with MICs all greater than 1000 μg mL^{-1} under identical test conditions. Therefore, the antimicrobial property of Gua-POSS supramolecules should be ascribed to the multiple salt bridges and hydrogen bonds formed between the positive guanidinium and negative phosphates on the microbial membrane (Figure 1b).[27−29] In addition, the guanidinium groups need to be spatially organized to facilitate the antimicrobial action, evidenced by the fact that free-standing guanidinium (**C3**, Figure 1a) does not display any antimicrobial effect up to 1000 μg mL^{-1}. This finding echoes a previous report by Böttcher et al. that guanidinium groups have to be precisely spaced on linear molecules to exert strong antimicrobial activity.[28]

To study the detailed effects of Gua-POSS on the microbial membrane, fluorescence staining assays using propidium iodide (PI) dyes were conducted to monitor the membrane permeability. The DNA-binding PI dye remains silent in the presence of microbes with intact membranes but exhibits strong fluorescence if the membrane is disrupted.[43] As shown in Figure 2a, Gua-POSS treatment on *E. coli* at 125 μg mL^{-1} (at or below their MBCs over 1 h, Figures S2−S4) led to dramatic fluorescence increase, suggesting that the cationic Gua-POSS supramolecules are able to penetrate through the pores across the bacterial cell wall and induce significant membrane disruption.[44,45] Among the different Gua-POSS designs, **T10-C1**, **T10-C3**, and **T8-C3** induce similar fluorescence increases upon mixing with the bacteria, and their effects are comparable to that of polymyxin B, an antibiotic against Gram-negative bacteria well known for its capability to form pinholes on the membrane.[24] In comparison, **T8-C1** demonstrates a much lower activity in disrupting the *E. coli* membrane but still significantly higher than the negative control. Using an identical PI fluorescence assay, similar disruptive effects were also observed on the cytoplasmic membranes of *S. aureus* (Figure 2b) and *C. albicans* (Figure 2c), suggesting the general capability of these Gua-POSS supramolecules to disrupt microbial membranes and the effect is dependent on the actual structural design. Such structure-dependent membrane disruption was consistently observed at lower Gua-POSS concentrations of 62.5 and 31.3 μg mL^{-1} (below their MBCs over 1 h), and a good correlation can be established between the membrane disruption and microbes killing (Figures S2−S4), implying that membrane disruption, instead of translocation,[11] is the primary antimicrobial mechanism of these Gua-POSS supramolecules. In addition, different membrane permeabilities of Gua-POSS to respective microbial species are likely due to the distinct cell surface structures and compositions.

To attain visual confirmation on the membrane damage, field emission scanning electron microscopy (FESEM) images were taken on the microbial cells with and without Gua-POSS treatment. As a conservative example, **T8-C1**, the least membrane-disrupting Gua-POSS identified by the aforementioned fluorescence assays, induced significant membrane lysis on *E. coli* cells (Figure 2d). Many "broken" or "deflated" cells were observed after the treatment, whereas the untreated control retained their original intact ellipsoidal cellular morphology. Similar phenomenon was also observed on *S. aureus* and *C. albicans* (Figure 2e,f), as well as using other Gua-POSS designs (Figure S5). We further note that such a membrane-targeting antimicrobial mechanism is not reliant on any metabolism or proliferation process, thus making it unlikely for the microbes to develop resistance.[11]

https://doi.org/10.1021/acsami.2c16493
ACS Appl. Mater. Interfaces 2023, 15, 354−363

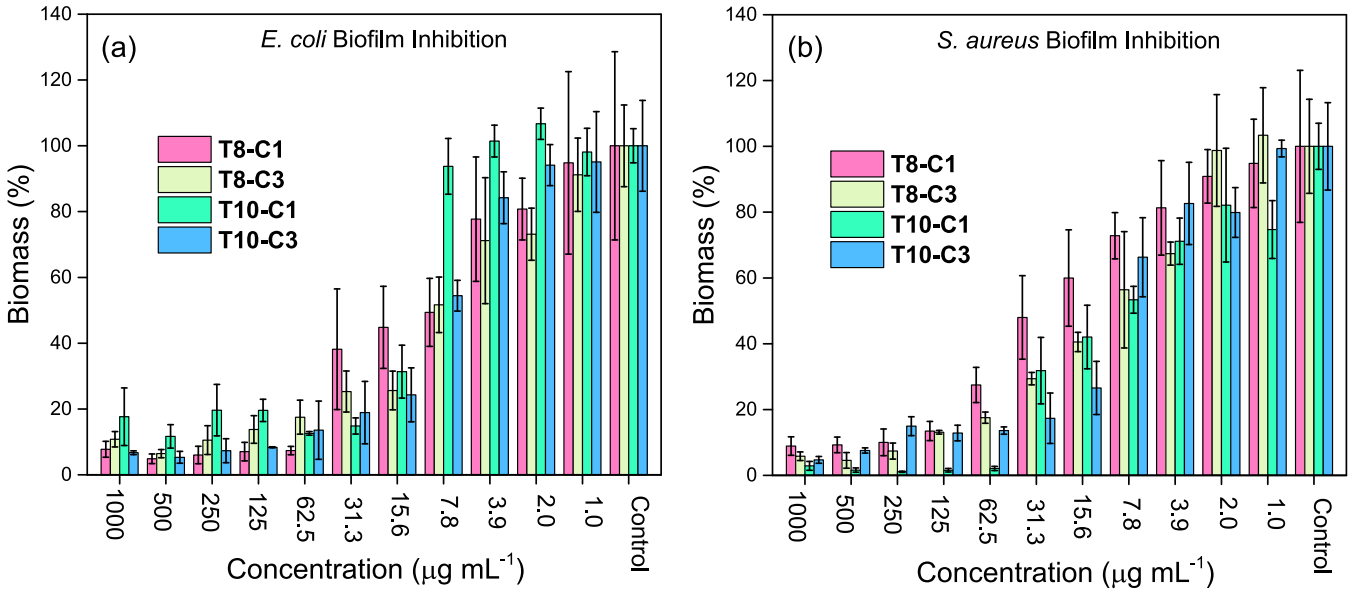

Figure 3. Biomass inhibition efficacy of Gua-POSS supramolecules against (a) Gram-negative *E. coli* and (b) Gram-positive *S. aureus* biofilm formation. $MBIC_{50}$ against *E. coli* are in the 7.8−15.6 μg mL^{-1} range, and $MBIC_{50}$ against *S. aureus* are in the range of 15.6−31.3 μg mL^{-1}. Each test was repeated three times, and the average value is reported with standard deviation as error bars.

2.4. *In Vitro* Hemolytic Activity and Cytotoxicity. The *in vitro* hemolytic activity and cytotoxicity of Gua-POSS molecules were measured to evaluate their cytocompatibility for future clinical applications. As shown in Figure S6, all four Gua-POSS supramolecular designs exhibit negligible hemolytic activities against rat red blood cells with concentrations up to 2000 μg mL^{-1} in PBS. Upon close inspection, those with T10 cores demonstrated slightly higher hemolytic activities than their analogues with T8, though all were below 5% across the 3.9−2000 μg mL^{-1} concentration range tested.

In vitro cytotoxicity of these Gua-POSS supramolecules was assessed on L929 mouse fibroblast cells using the alamar Blue cell viability assay (Figure S7), and their IC_{50} values were calculated to be 337.6, 426.6, 574.4, and 584.4 μg mL^{-1} for **T10-C1**, **T10-C3**, **T8-C1**, and **T8-C3**, respectively. They are much higher than the above-shown antimicrobial MICs/MBCs/MFCs, and the large differences are therefore indicative of Gua-POSS's good selectivity toward microbial cells over mammalian cells. This could be ascribed to the intrinsic difference in their cellular membrane structures, wherein the microbial membrane carries negative charges, while mammalian cells are mostly neutral.

2.5. Inhibition of Biofilm Formation. Many bacteria tend to form biofilms on living or nonliving surfaces, posing a critical threat in healthcare, municipal, and industrial settings.[46] Protected by the ECM, bacteria encased in biofilms are much less susceptible to antibiotics and conventional antimicrobial therapies, making it an imperative task to develop effective anti-biofilm strategies. Using biomass staining assays,[47] we found that all our Gua-POSS supramolecules display significant and comparable biofilm inhibitory effects against both Gram-negative *E. coli* and Gram-positive *S. aureus* strains (Figure 3). The minimum biofilm inhibitory concentration ($MBIC_{50}$, defined as the lowest concentration at which at least 50% of biofilm biomass formation is inhibited relative to the untreated control)[22] of Gua-POSS against *E. coli* biofilm formation was determined to be 7.8−15.6 μg mL^{-1}. Similar inhibitory performance was also observed on Gram-positive *S. aureus*, with $MBIC_{50}$ in the 15.6−31.3 μg mL^{-1} range. At a concentration of 125 μg mL^{-1} or higher, more than 80% of the biofilm formation from both bacteria can be prevented by Gua-POSS in a single treatment.

2.6. Disruption of Preestablished Biofilms. In addition to biofilm inhibition, the capability of these Gua-POSS supramolecules to break down and remove preestablished biofilms was also experimentally verified. Using the biomass staining assay,[47] all four Gua-POSS supramolecules were found to be highly effective in breaking down the preformed *S. aureus* biofilms at different maturity stages (Figure 4). For example, **T10-C3** at a concentration of 1000 μg mL^{-1} is able to eradicate 94.0% of young *S. aureus* biofilms. For mediate and mature *S. aureus* biofilms, the disruption/removal efficacies are 96.8 and 100%. At a lower concentration of 250 μg mL^{-1} (∼50 μM), the biomass removal efficacies of **T10-C3** were 84.2, 84.6, and 85.2% for young, mediate, and mature *S. aureus* biofilms, respectively. In addition, the XTT assay was subsequently employed to quantify the viability of bacterial cells in the biomass residual. In principle, metabolically active bacterial cells can reduce the colorless XTT probe, 2,3-bis(2-methoxy-4-nitro-5-sulfophenyl)-5-[(phenylamino)carbonyl]-2*H*-tetrazolium hydroxide, into a water-soluble formazan with bright orange color, and the color intensity is linearly proportional to the number of viable cells present. As shown in Figure 4d−f, almost no viable *S. aureus* cells were detected in the residual biomass of different-aged biofilms after Gua-POSS treatment at 1000 μg mL^{-1} concentration. In other words, the biomass residual observed mainly consisted of cellular debris and dead bacteria instead of viable ones.

Visual confirmation was obtained by FESEM images taken on *S. aureus* biofilms with and without treatment, wherein a significant decrease in the amount of biofilm biomass was observed (Figures 4g−i and S8). Upon close inspection, most residual bacterial cells exhibited abnormal cellular morphology and significant membrane disruption (inset to Figure 4g2−i2), indicating that they are no longer viable. This observation is in good accordance with the biomass staining and XTT assay

https://doi.org/10.1021/acsami.2c16493
ACS Appl. Mater. Interfaces 2023, 15, 354−363

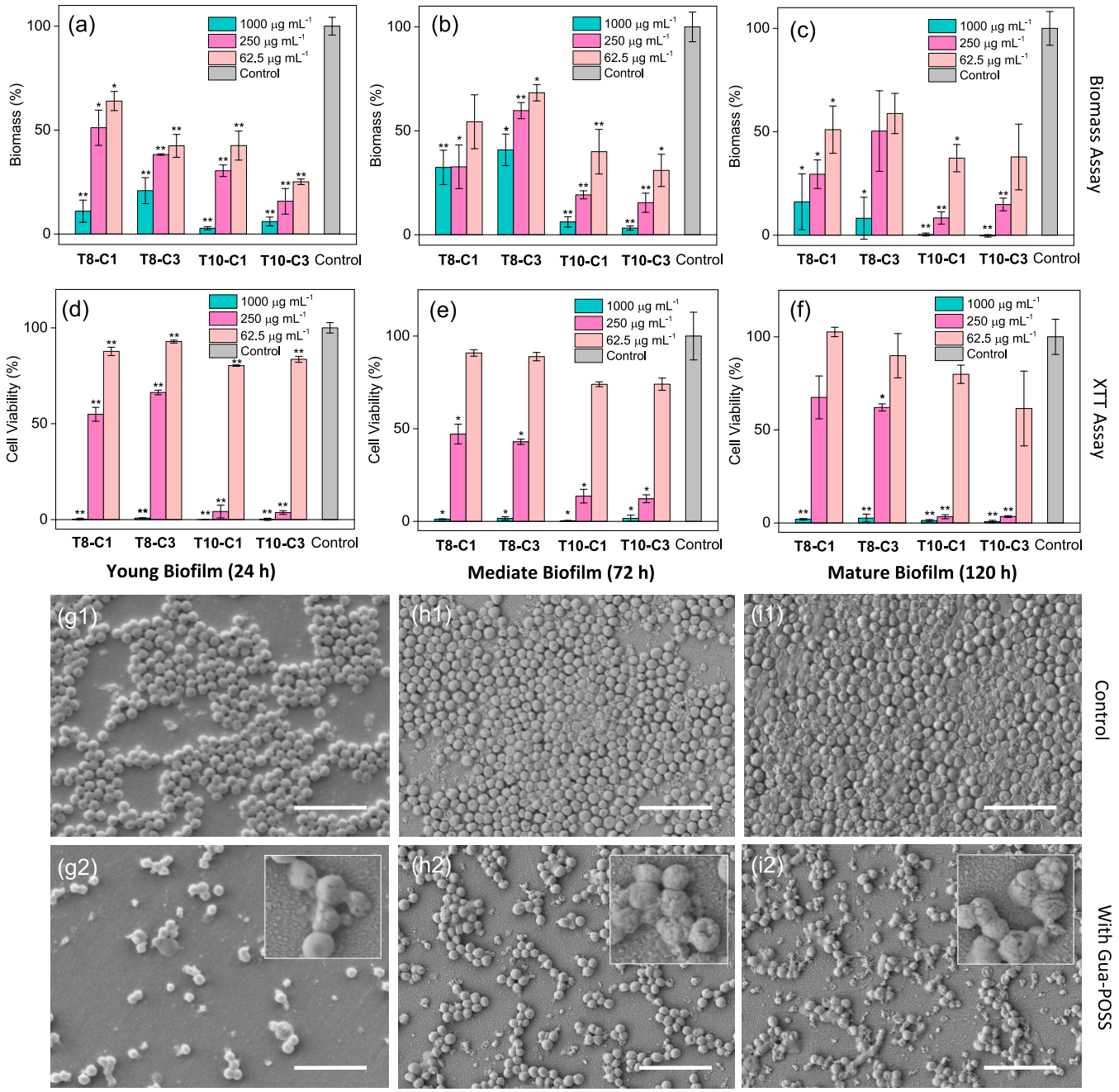

Figure 4. Disruption of preestablished *S. aureus* biofilms by Gua-POSS supramolecules: (a–c) biomass staining assay results, and (d–f) XTT cell viability assay results for young (left panels), mediate (middle panels), and mature (right panels) *S. aureus* biofilms. Three replicates were measured for each sample, and the results were expressed as the average value with standard deviation shown as the error bar. Statistically significant differences are indicated by $^{**}p < 0.01$ and $^{*}p < 0.05$, Student's *t*-test, compared with the negative control. (g–i) FESEM images of control (top panels) *S. aureus* biofilms at different maturity stages and those treated with 1000 μg mL^{-1} **T10-C3** overnight at 37 °C (bottom panels). Scale bar is 5 μm. Insets show the disrupted microbial membranes of the residual *S. aureus* cells. Other Gua-POSS all demonstrate similar biofilm disruption and removal effect (see Figure S8).

results shown above. At a lower concentration of 62.5 μg mL^{-1}, partial biofilm disruption and removal by Gua-POSS can still be observed (Figure 4a–f). It is worth noting that T10-based Gua-POSS are in general more potent than the T8-based ones, in line with the trend of their antimicrobial MBCs. This implies that for such large spherical molecules, the number of peripheral functional groups and their 3D spatial arrangement are important in determining the apparent anti-biofilm activities. Similar biofilm disruption and removal performances were also recorded on *E. coli* biofilms (Figure S9), indicating the general anti-biofilm capability of Gua-POSS supramolecules with precise well-defined spherical structures.

2.7. Antiviral Activity against Coronavirus. In view of the inhibitory effect of guanidine derivatives against coronavirus,[48] we expect our Gua-POSS supramolecules to exhibit antiviral activities too. The BSL-2 murine hepatitis coronavirus (MHV, ATCC VR-764TM), a mice-infecting enveloped positive-sense RNA coronavirus, was used as a surrogate for the real SARS-CoV species, due to its high structural similarities.[49]

https://doi.org/10.1021/acsami.2c16493
ACS Appl. Mater. Interfaces 2023, 15, 354–363

The antiviral performance against MHV was experimentally quantified using plaque-counting assays on confluent monolayers of NCTC clone 1469 mouse liver cells.[50] As shown in Table 2, both **T10-C3** and **T8-C1** at 0.5 wt % displayed excellent antiviral efficacy exceeding the limit of detection (*i.e.*, 99.9%), which were significantly higher than those of **T10-C1** and **T8-C3** showing efficacies of 93.3 and 78.5%, respectively. Upon lowering the concentration to 0.1 wt %, good antiviral efficacies can still be observed with more than 95% of the coronavirus inactivated by **T10-C3** and **T8-C1** after 1 h incubation. The killing kinetics was then established using different incubation durations (Table S1). **T8-C1** at 0.5 wt % was found capable of deactivating 99.5 and 98.2% of the coronavirus after 30 and 10 min incubations, respectively, in media, whereas **T10-C3** demonstrated a slightly lower activity, registering at 99.3 and 93.2% for 30 and 10 min incubations at identical test conditions, respectively.

Table 2. Antiviral Efficacies of Different Gua-POSS Supramolecular Designs against Murine Hepatitis Virus (MHV)[a]

	0.5 wt %	0.2 wt %	0.1 wt %
T10-C1	93.3 ± 0.7%		
T10-C3	>99.9%	97.4 ± 1.0%	96.9 ± 1.0%
T8-C1	>99.9%	99.7 ± 0.05%	95.1 ± 1.5%
T8-C3	78.5 ± 3.7%		

[a]The incubation period was 1 h at room temperature. The test was conducted inside a BSL-2 hood, and each condition was conducted in three parallel replicates.

We note that the plaque reduction can be caused by two different mechanisms, including virus inactivation and host cell protection. A control experiment was hence performed to disentangle these two possibilities, wherein the confluent monolayer of host cells was pretreated with **T8-C1** (as a representative of the Gua-POSS family) for 1 h, followed by washing with PBS and then subject to MHV infection. The result showed similar number of plaques to the negative control, implying that Gua-POSS supramolecules have no protective effect on the host cells and the plaque reduction was indeed caused by virus inactivation. In general, negatively charged regions can be universally found on the virus surface proteins, and the cationic Gua-POSS could interact with such regions through electrostatic interaction, thus masking the virus from cell infection (a common antiviral mechanism for cationic polymers).[51] Another possible antiviral mechanism could be disruption of the viral membranes by the Gua-POSS supramolecules, similar to the antibacterial mechanism described above, although the specific interactions could be different, evidenced by the fact that the superiority of T10-based Gua-POSS over T8 ones was not seen. It is worth further noting that the lipid envelope of the real SARS-CoV-2 is thinner than that of MHV (3.9 *vs* 7.6 nm),[52] making the former usually more susceptible to antiviral agents.[50] An even higher anti-SARS-CoV-2 efficacy can therefore be expected from our Gua-POSS supramolecular designs.[50]

3. CONCLUSIONS

We have successfully conceptualized a novel class of modularly structured guanidinium-perfunctionalized polyhedral oligomeric silsesquioxane (Gua-POSS) supramolecules with atomic precision and demonstrated their highly potent antimicrobial activities. These spherical Gua-POSS supramolecules can effectively act against Gram-positive bacteria (*S. aureus*), Gram-negative bacteria (*E. coli*), and fungal species (*C. albicans*) via the membrane disruption mechanism with MICs of 1.7−6.8 μM in media. More importantly, they can inhibit the biofilm formation at concentrations around their MICs, and break down preestablished biofilms of varying maturity stages at ∼50 μM. They are also capable of inactivating the enveloped coronavirus, with the best-performer able to reduce >99.9% of the viral count within 1 h and >98.2% within just 10 min. Our findings thus demonstrate that the cytocompatible POSS could be employed as a structurally well-defined scaffold to construct antimicrobials with excellent biocidal activities, offering a novel design approach to structurally distinctive inorganic−organic hybrid supramolecules for diverse healthcare, municipal, and industrial applications.

4. EXPERIMENTAL SECTION

4.1. Materials. All chemicals were purchased from commercial sources and used as received unless otherwise stated. *S. aureus* (ATCC 6538), *E. coli* (ATCC 25922), and *C. albicans* (ATCC 10231) were purchased from ATCC and reconstituted based on the recommended protocols. Mueller−Hinton broth (MHB) was purchased from BD Diagnostics (Singapore) and was prepared according to the instructions from the manufacturer. NCTC clone 1469 cells were purchased from CLS Cell Lines Service GmbH and maintained in a 37 °C, 5% CO_2 incubator, in Dulbecco's Modified Eagle's Medium (DMEM) supplemented with 10% horse serum and 1% penicillin−streptomycin. Murine hepatitis virus (MHV, ATCC VR-764TM) was a kind donation from Yee Joo Tan (Institute of Molecular and Cell Biology, A*STAR, Singapore).

4.2. Syntheses and Characterizations of Gua-POSS. Details of synthetic steps, NMR spectra, and ESI-MS data can be found in the Supporting Information.

4.3. MIC and MBC Measurements. The minimum inhibitory concentration (MIC) of Gua-POSS was measured using the broth microdilution method.[53] In brief, bacteria/fungi were first cultured overnight at appropriate temperatures (*i.e.*, 37 °C for bacteria, room temperature for fungus) in Mueller−Hinton broth (MHB) to enter its log growth phase. The concentration of bacterial or fungal solution was adjusted to have an initial optical density (OD) reading of ∼0.07 at 600 nm on a microplate reader (Tecan, Switzerland), which corresponds to a concentration of Mcfarland 1 solution (∼3 × 10^8 CFU mL^{-1}). The solution was then further diluted 1000-fold to achieve an initial inoculum of ∼3 × 10^5 CUF mL^{-1}. MHB media (100 μL) containing Gua-POSS (with a fixed DI water concentration of 20%, v/v) at various concentrations (0−1000 μg mL^{-1}) was loaded into each well of a 96-well microplate. An equal volume of microbial suspension (∼3 × 10^5 CFU mL^{-1}) in MHB was added into each well. The plate of bacteria was kept in an incubator at 37 °C under constant shaking of 300 rpm for 24 h, and the plate of fungus was incubated at room temperature for 48 h. The MIC was defined as the lowest concentration at which there was no microbial growth observed with naked eyes and the microplate reader. MHB media containing microbial cells alone was used as the negative control, and each test was conducted with six parallel replicates. The suspension with no microbial growth was spread on agar plates for quantification, and MBC was determined as the lowest concentration wherein >99.9% of microbes were killed. Each test was repeated three times, and similar results were obtained.

4.4. Hemolysis Assay. The hemolytic activity of Gua-POSS was tested using fresh rat red blood cells (rRBCs). In brief, fresh rRBCs were diluted 30-fold in PBS to achieve 3.3% v/v of blood content. The Gua-POSS were dissolved in PBS with a concentration range of 0−4000 μg mL^{-1}. Equal volume of Gua-POSS solution was then mixed with the diluted blood sample (100 μL each). The mixtures were then incubated at 37 °C for 1 h to allow for a thorough

https://doi.org/10.1021/acsami.2c16493
ACS Appl. Mater. Interfaces 2023, 15, 354−363

interaction between rRBCs and Gua-POSS supramolecules. Afterward, the mixture was subject to centrifugation (1000*g* for 5 min, 4 °C), and 100 μL aliquots of the supernatant were transferred into a 96-well microplate. The hemoglobin release was measured spectrophotometrically by recording the absorbance at 576 nm using the microplate reader (Tecan, Switzerland). Two control groups were employed for this assay: untreated rRBC suspension as the negative control and rRBC suspension treated with 0.8% Triton-X as the positive control. The percentage of hemolysis was defined as Hemolysis (%) = [(OD_{576} of the treated sample − OD_{576} of the negative control)/(OD_{576} of the positive control − OD_{576} of the negative control)] × 100%. Each assay was performed in four parallel replicates, and the average values were reported with standard deviations shown as error bars.

4.5. Cell Viability Test. *In vitro* cytotoxicity of Gua-POSS was tested against L929 mouse fibroblast cells. In brief, ∼5 × 10^3 cells were first seeded into wells of a black 96-well plate and incubated for 24 h at 37 °C. Gua-POSS was dissolved in media with a 2-fold dilution to reach the desired concentrations. The spent media above the seeded cell monolayer was removed carefully, followed by adding 100 μL of the Gua-POSS solution to each well. After incubation for another 24 h at 37 °C, the Gua-POSS solution was removed, and 100 μL alamar blue and DMEM mixture (1:9, v/v) was added in each well. After 3 h incubation at 37 °C, the fluorescence intensity of alamar blue was recorded using a microplate reader (Tecan, Switzerland) with 560 nm excitation and 590 nm emission wavelengths. Two controls were used in this assay: cells with alamar blue and alamar blue only. The percentage of cell viability was defined as Viability (%) = [(F_{590} of the Gua-POSS treated well − F_{590} of alamar blue only)/(F_{590} of untreated cells with alamar blue − F_{590} of alamar blue only)] × 100%. Each assay was performed in three parallel replicates, and the average values were reported with standard deviations shown as error bars.

4.6. PI Assay to Monitor Microbial Membrane Permeability. The membrane permeability assay using propidium iodide (PI) dye was performed according to literature procedures.[43] In brief, bacteria (*E. coli* and *S. aureus*, incubated at 37 °C) and fungus (*C. albicans*, incubated at room temperature) were grown for 24 h in MHB before being harvested, washed, and resuspended in a buffer solution containing 5 mM glucose and 5 mM HEPES at pH 7.2 to an OD_{600nm} value of ∼0.25. Such a microbial suspension (150 μL) was added to wells of a black 96-well plate. PI solution (50 μM, 10 μL, in sterile water) was added and preincubated for 10 min. Following preincubation, fluorescence was measured for the next 8 min with a time interval of 2 min using a microplate reader (535 nm excitation, 617 nm emission, Tecan, Switzerland). Gua-POSS at desired concentrations was added, and the fluorescence intensity was monitored with a time interval of 2 min. For the bacterial/fungal quantification after Gua-POSS treatment, the treated microbial suspension was serially diluted in PBS and plated on an agar plate for colony counting the next day. Each test was performed in three parallel replicates, and the average values were reported with standard deviations shown as the error bars.

4.7. FESEM Imaging. Bacteria or fungus cells in MHB media with and without Gua-POSS treatment were incubated at 37 °C (for bacteria) or room temperature (for fungus) overnight. All microbial suspensions were collected into a microfuge tube and pelleted at 4000 rpm for 5 min at room temperature and then washed twice with PBS. Subsequently, cell fixing with formalin solution (10% neutral buffered) for 2 h was conducted, followed by washing with DI water twice. Dehydration of the cells was performed using a series of ethanol/water mixtures (25, 50, 70, 90, and 100%). The dehydrated samples were dried at room temperature overnight and coated with Pt (JEOL JFC-1600 high-resolution sputter coater) before FESEM imaging on a JEOL JSM-7400F (Japan) setup. Biofilm samples for FESEM imaging were prepared using similar approaches. In brief, bacteria were grown in a 96-well plate for 24−120 h and then treated with Gua-POSS, after which the biofilm formed was washed with PBS, fixed with formalin, dehydrated using ethanol/water mixtures, and dried in air before imaging.

4.8. Biofilm Inhibition Assay. *S. aureus* and *E. coli* were cultured in Mueller−Hinton broth (MHB) at 37 °C overnight. The bacterial suspension was diluted using fresh MHB to reach OD_{600nm} ∼ 0.07. Such a bacterial suspension (100 μL) was mixed with 100 μL of Gua-POSS solution of desired concentration in wells of a transparent 96-well plate, followed by incubation at 37 °C for 24 h. The spent media was removed, and the biofilm formed was washed with 200 μL of PBS thrice to remove planktonic cells. Crystal violet staining assay was used to quantify the biofilm biomass. In brief, 200 μL of methanol was added to each well to fix the biomass for 15 min, followed by adding 200 μL of crystal violet solution (1%, w/v) and incubated for another 10 min for staining. The excess crystal violet was washed away with DI water. The crystal violet bound with the biomass was extracted by 33% glacial acetic acid (200 μL) and absorbance at 570 nm was recorded using the microplate reader (Tecan, Switzerland). Each test condition was conducted in three parallel replicates. The results were expressed as a percentage relative to the control biomass without Gua-POSS treatment, and standard deviations were shown as the error bars.

4.9. Biofilm Disruption and Removal Assay. *S. aureus* and *E. coli* were cultured in Mueller−Hinton broth (MHB) at 37 °C overnight. The bacterial suspension was diluted using fresh MHB to reach OD_{600nm} ∼ 0.07. The bacterial suspension (125 μL) was loaded into each well of a transparent 96-well microplate followed by incubation at 37 °C for 24 h. The spent media was removed and the biofilms were washed with PBS to remove planktonic cells before adding in another 125 μL fresh MHB media for a new cycle of biofilm development. After the desired incubation period, the biofilms were thoroughly washed with PBS, and Gua-POSS solution at the desired concentration in MHB/water mixture (9:1, v/v) was then added to each well, followed by incubation for another 24 h at 37 °C for biofilm disruption. At the end of the treatment, the remaining biofilm biomass was quantified using the crystal violet staining assay as described above. In addition, XTT assay was also employed to quantify the cell viability in the residual biomass. Such XTT assay is based on the reduction of 2,3-bis(2-methoxy-4-nitro-5-sulfophenyl)-5-[(phenylamino)carbonyl]-2*H*-tetrazolium hydroxide (XTT) by metabolically active microbial cells to water-soluble formazan with bright orange color. In brief, XTT solution was prepared using PBS (1 mg mL^{-1}) and filtered with PVDF filter of 0.45 μm pore size. Menadione solution (0.4 mM) was prepared in acetone and freshly mixed with the XTT solution at a volume ratio of 1:5 before use. At the end of the Gua-POSS treatment, the spent media was removed and the biofilms were washed with PBS thrice to remove planktonic cells. Then, 120 μL of PBS and 14.4 μL of the XTT-menadione mixture solution was added to each well and incubated for 6 h in dark. An aliquot of 100 μL was then taken and transferred to a fresh transparent 96-well plate. Absorbance at 490 nm was recorded with a microplate reader (Tecan, Switzerland). The results were expressed as a percentage of viable cells in the control biofilm without Gua-POSS treatment. Each test was performed in three parallel replicates, and the average values were reported with standard deviations shown as the error bars.

4.10. Antiviral Test. The antiviral activity was quantified using a plaque-counting assay. NCTC clone 1469 cells were purchased from CLS and cultured in Dulbecco's Modified Eagle's Medium (DMEM, Invitrogen GIBCO) containing 4500 mg L^{-1}, D-glucose, and L-glutamine supplemented with 10% horse serum, 100 U mL^{-1} penicillin, and 100 μg mL^{-1} streptomycin at 37 °C in 5% CO_2 atmosphere. Infection of the NCTC clone 1469 cells by MHV was conducted in DMEM with 2% horse serum. Briefly, NCTC clone 1469 cells were first seeded in a transparent 6-well plate, with ∼1 × 10^6 cells per well, followed by incubating at 37 °C with 5% CO_2 atmosphere overnight to form the confluent cell monolayer. Then, 50 μL of the murine hepatitis virus suspension (∼10^7 PFU mL^{-1}) was mixed with 950 μL of Gua-POSS solution in sterile water and incubated for a desired period at room temperature. Pure sterile water was used as the negative control. The viral suspension was then subject to 10-fold serial dilutions in media. Infection of the host cells was done by inoculating 500 μL of the diluted viral suspension to a

https://doi.org/10.1021/acsami.2c16493
ACS Appl. Mater. Interfaces 2023, 15, 354−363

confluent monolayer of NCTC clone 1469 cells preseeded in 6-well plates. The inoculated monolayer was kept in an incubator at 37 °C, 5% CO_2 for 1 h with tilting of the plates every 15 min to keep the cell monolayer moist. Following 1 h incubation, 2.5 mL of warm agarose medium (0.8% w/v in DMEM) was added into each well and allowed to solidify before incubating the plates at 37 °C in 5% CO_2 atmosphere for another 2 days. The cells were then fixed by 10% formalin solution at room temperature for 3 h before removing the solidified agar and staining with 5% crystal violet solution for plaque-counting. Each test was performed in three parallel replicates, and the average values and standard deviations were reported.

■ ASSOCIATED CONTENT

Supporting Information

The Supporting Information is available free of charge at https://pubs.acs.org/doi/10.1021/acsami.2c16493.

Details of Gua-POSS synthetic procedures, characterizations, and supplementary experimental data (PDF)

■ AUTHOR INFORMATION

Corresponding Authors

Ning Li − *Institute of Bioengineering and Bioimaging, A*STAR, Singapore 138669*; orcid.org/0000-0003-0179-1425; Email: li_ning@ibb.a-star.edu.sg

Huaqiang Zeng − *College of Chemistry, Fuzhou University, Fuzhou, Fujian 350116, China*; Email: hqzeng@fzu.edu.cn

Yi Yan Yang − *Institute of Bioengineering and Bioimaging, A*STAR, Singapore 138669*; orcid.org/0000-0002-1871-5448; Email: yyyang@ibb.a-star.edu.sg

Authors

He-Kuan Luo − *Institute of Sustainability for Chemicals, Energy and Environment, A*STAR, Singapore 627833*

Adrielle Xianwen Chen − *Institute of Bioengineering and Bioimaging, A*STAR, Singapore 138669*

Jeremy Pang Kern Tan − *Institute of Bioengineering and Bioimaging, A*STAR, Singapore 138669*

Chuan Yang − *Institute of Bioengineering and Bioimaging, A*STAR, Singapore 138669*

Melgious Jin Yan Ang − *Institute of Bioengineering and Bioimaging, A*STAR, Singapore 138669*

Complete contact information is available at: https://pubs.acs.org/10.1021/acsami.2c16493

Author Contributions

The manuscript was written through contributions of all authors. All authors have given approval to the final version of the manuscript.

Notes

The authors declare no competing financial interest.

■ ACKNOWLEDGMENTS

The authors gratefully acknowledge the Singapore AME Young Individual Research Grant (A2084c0174) and the Institute of Bioengineering and Bioimaging (IBB, Biomedical Research Council, Agency for Science, Technology and Research, Singapore) for financial support.

■ REFERENCES

(1) Baker, R. E.; Mahmud, A. S.; Miller, I. F.; Rajeev, M.; Rasambainarivo, F.; Rice, B. L.; Takahashi, S.; Tatem, A. J.; Wagner, C. E.; Wang, L.-F.; Wesolowski, A.; Metcalf, C. J. E. Infectious disease in an era of global change. *Nat. Rev. Microbiol.* **2022**, *20*, 193−205.

(2) Cully, M. Public health: The politics of antibiotics. *Nature* **2014**, *509*, S16−S17.

(3) Nathan, C. Resisting antimicrobial resistance. *Nat. Rev. Microbiol.* **2020**, *18*, 259−260.

(4) Fisher, R. A.; Gollan, B.; Helaine, S. Persistent bacterial infections and persister cells. *Nat. Rev. Microbiol.* **2017**, *15*, 453−464.

(5) Makabenta, J. M. V.; Nabawy, A.; Li, C.-H.; Schmidt-Malan, S.; Patel, R.; Rotello, V. M. Nanomaterial-based therapeutics for antibiotic-resistant bacterial infections. *Nat. Rev. Microbiol.* **2021**, *19*, 23−36.

(6) Kalelkar, P. P.; Riddick, M.; García, A. J. Biomaterial-based antimicrobial therapies for the treatment of bacterial infections. *Nat. Rev. Mater.* **2022**, *7*, 39−54.

(7) Bush, K.; Courvalin, P.; Dantas, G.; Davies, J.; Eisenstein, B.; Huovinen, P.; Jacoby, G. A.; Kishony, R.; Kreiswirth, B. N.; Kutter, E.; Lerner, S. A.; Levy, S.; Lewis, K.; Lomovskaya, O.; Miller, J. H.; Mobashery, S.; Piddock, L. J. V.; Projan, S.; Thomas, C. M.; Tomasz, A.; Tulkens, P. M.; Walsh, T. R.; Watson, J. D.; Witkowski, J.; Witte, W.; Wright, G.; Yeh, P.; Zgurskaya, H. I. Tackling antibiotic resistance. *Nat. Rev. Microbiol.* **2011**, *9*, 894−896.

(8) Mah, T.-F.; Pitts, B.; Pellock, B.; Walker, G. C.; Stewart, P. S.; O'Toole, G. A. A genetic basis for Pseudomonas aeruginosa biofilm antibiotic resistance. *Nature* **2003**, *426*, 306−310.

(9) Hutchings, M. I.; Truman, A. W.; Wilkinson, B. Antibiotics: past, present and future. *Curr. Opin. Microbiol.* **2019**, *51*, 72−80.

(10) Zasloff, M. Antimicrobial peptides of multicellular organisms. *Nature* **2002**, *415*, 389−395.

(11) Chin, W.; Zhong, G.; Pu, Q.; Yang, C.; Lou, W.; De Sessions, P. F.; Periaswamy, B.; Lee, A.; Liang, Z. C.; Ding, X.; Gao, S.; Chu, C. W.; Bianco, S.; Bao, C.; Tong, Y. W.; Fan, W.; Wu, M.; Hedrick, J. L.; Yang, Y. Y. A macromolecular approach to eradicate multidrug resistant bacterial infections while mitigating drug resistance onset. *Nat. Commun.* **2018**, *9*, No. 917.

(12) Wu, Y.; Lin, Y.; Cong, Z.; Chen, K.; Xiao, X.; Wu, X.; Liu, L.; She, Y.; Liu, S.; Zhou, R.; Yin, G.; Shao, X.; Dai, Y.; Lin, H.; Liu, R. Peptide Polymer-Doped Cement Acting as an Effective Treatment of MRSA-Infected Chronic Osteomyelitis. *Adv. Funct. Mater.* **2022**, *32*, No. 2107942.

(13) Qian, Y.; Deng, S.; Cong, Z.; Zhang, H.; Lu, Z.; Shao, N.; Bhatti, S. A.; Zhou, C.; Cheng, J.; Gellman, S. H.; Liu, R. Secondary Amine Pendant β-Peptide Polymers Displaying Potent Antibacterial Activity and Promising Therapeutic Potential in Treating MRSA-Induced Wound Infections and Keratitis. *J. Am. Chem. Soc.* **2022**, *144*, 1690−1699.

(14) Xie, J.; Zhou, M.; Qian, Y.; Cong, Z.; Chen, S.; Zhang, W.; Jiang, W.; Dai, C.; Shao, N.; Ji, Z.; Zou, J.; Xiao, X.; Liu, L.; Chen, M.; Li, J.; Liu, R. Addressing MRSA infection and antibacterial resistance with peptoid polymers. *Nat. Commun.* **2021**, *12*, No. 5898.

(15) Sun, J.; Li, M.; Lin, M.; Zhang, B.; Chen, X. High Antibacterial Activity and Selectivity of the Versatile Polysulfoniums that Combat Drug Resistance. *Adv. Mater.* **2021**, *33*, No. 2104402.

(16) Huang, Y.; Hu, C.; Zhou, Y.; Duan, R.; Sun, Z.; Wan, P.; Xiao, C.; Pang, X.; Chen, X. Monomer Controlled Switchable Copolymerization: A Feasible Route for the Functionalization of Poly(lactide). *Angew. Chem., Int. Ed.* **2021**, *60*, 9274−9278.

(17) Locock, K. E. S.; Michl, T. D.; Valentin, J. D. P.; Vasilev, K.; Hayball, J. D.; Qu, Y.; Traven, A.; Griesser, H. J.; Meagher, L.; Haeussler, M. Guanylated Polymethacrylates: A Class of Potent Antimicrobial Polymers with Low Hemolytic Activity. *Biomacromolecules* **2013**, *14*, 4021−4031.

(18) Sahariah, P.; Cibor, D. A.-O.; Zielińska, D.; Hjálmarsdóttir, M.; Stawski, D. A.-O.; Másson, M. A.-O. The Effect of Molecular Weight on the Antibacterial Activity of N,N,N-Trimethyl Chitosan (TMC). *Int. J. Mol. Sci.* **2019**, *20*, 1743.

(19) Tyagi, A.; Mishra, A. Optimal Balance of Hydrophobic Content and Degree of Polymerization Results in a Potent Membrane-Targeting Antibacterial Polymer. *ACS Omega* **2021**, *6*, 34724−34735.

(20) Mowery, B. P.; Lindner, A. H.; Weisblum, B.; Stahl, S. S.; Gellman, S. H. Structure−activity Relationships among Random

Nylon-3 Copolymers That Mimic Antibacterial Host-Defense Peptides. *J. Am. Chem. Soc.* **2009**, *131*, 9735−9745.
(21) Joseph, R.; Kaizerman, D.; Herzog, I. M.; Hadar, M.; Feldman, M.; Fridman, M.; Cohen, Y. Phosphonium pillar[5]arenes as a new class of efficient biofilm inhibitors: importance of charge cooperativity and the pillar platform. *Chem. Commun.* **2016**, *52*, 10656−10659.
(22) Joseph, R.; Naugolny, A.; Feldman, M.; Herzog, I. M.; Fridman, M.; Cohen, Y. Cationic Pillararenes Potently Inhibit Biofilm Formation without Affecting Bacterial Growth and Viability. *J. Am. Chem. Soc.* **2016**, *138*, 754−757.
(23) Gao, L.; Li, M.; Ehrmann, S.; Tu, Z.; Haag, R. Positively Charged Nanoaggregates Based on Zwitterionic Pillar[5]arene that Combat Planktonic Bacteria and Disrupt Biofilms. *Angew. Chem., Int. Ed.* **2019**, *58*, 3645−3649.
(24) Guo, S.; Huang, Q.; Chen, Y.; Wei, J.; Zheng, J.; Wang, L.; Wang, Y.; Wang, R. Synthesis and Bioactivity of Guanidinium-Functionalized Pillar[5]arene as a Biofilm Disruptor. *Angew. Chem., Int. Ed.* **2021**, *60*, 618−623.
(25) Zhang, M.; Zhu, P.-P.; Xin, P.; Si, W.; Li, Z.-T.; Hou, J.-L. Synthetic Channel Specifically Inserts into the Lipid Bilayer of Gram-Positive Bacteria but not that of Mammalian Erythrocytes. *Angew. Chem., Int. Ed.* **2017**, *56*, 2999−3003.
(26) Wexselblatt, E.; Esko, J. D.; Tor, Y. On Guanidinium and Cellular Uptake. *J. Org. Chem.* **2014**, *79*, 6766−6774.
(27) Antonoplis, A.; Zang, X.; Huttner, M. A.; Chong, K. K. L.; Lee, Y. B.; Co, J. Y.; Amieva, M. R.; Kline, K. A.; Wender, P. A.; Cegelski, L. A Dual-Function Antibiotic-Transporter Conjugate Exhibits Superior Activity in Sterilizing MRSA Biofilms and Killing Persister Cells. *J. Am. Chem. Soc.* **2018**, *140*, 16140−16151.
(28) Böttcher, T.; Kolodkin-Gal, I.; Kolter, R.; Losick, R.; Clardy, J. Synthesis and Activity of Biomimetic Biofilm Disruptors. *J. Am. Chem. Soc.* **2013**, *135*, 2927−2930.
(29) Stanzl, E. G.; Trantow, B. M.; Vargas, J. R.; Wender, P. A. Fifteen Years of Cell-Penetrating, Guanidinium-Rich Molecular Transporters: Basic Science, Research Tools, and Clinical Applications. *Acc. Chem. Res.* **2013**, *46*, 2944−2954.
(30) Jiang, W.; Zhou, M.; Cong, Z.; Xie, J.; Zhang, W.; Chen, S.; Zou, J.; Ji, Z.; Shao, N.; Chen, X.; Li, M.; Liu, R. Short Guanidinium-Functionalized Poly(2-oxazoline)s Displaying Potent Therapeutic Efficacy on Drug-Resistant Fungal Infections. *Angew. Chem., Int. Ed.* **2022**, *61*, No. e202200778.
(31) Wender, P. A.; Galliher, W. C.; Goun, E. A.; Jones, L. R.; Pillow, T. H. The design of guanidinium-rich transporters and their internalization mechanisms. *Adv. Drug. Delivery Rev.* **2008**, *60*, 452−472.
(32) Li, N.; Chen, F.; Shen, J.; Zhang, H.; Wang, T.; Ye, R.; Li, T.; Loh, T. P.; Yang, Y. Y.; Zeng, H. Buckyball-Based Spherical Display of Crown Ethers for De Novo Custom Design of Ion Transport Selectivity. *J. Am. Chem. Soc.* **2020**, *142*, 21082−21090.
(33) Ye, R.; Ren, C.; Shen, J.; Li, N.; Chen, F.; Roy, A.; Zeng, H. Molecular Ion Fishers as Highly Active and Exceptionally Selective K + Transporters. *J. Am. Chem. Soc.* **2019**, *141*, 9788−9792.
(34) Li, N.; Shen, J.; Ang, G. K.; Ye, R.; Zeng, H. Molecular Tetrahedrons as Selective and Efficient Ion Transporters via a Two-Station Swing-Relay Mechanism. *CCS Chem.* **2021**, *3*, 2269−2279.
(35) Zeng, F.; Liu, F.; Yuan, L.; Zhou, S.; Shen, J.; Li, N.; Ren, H.; Zeng, H. A Pore-Forming Tripeptide as an Extraordinarily Active Anion Channel. *Org. Lett.* **2019**, *21*, 4826−4830.
(36) Majumdar, P.; Lee, E.; Gubbins, N.; Stafslien, S. J.; Daniels, J.; Thorson, C. J.; Chisholm, B. J. Synthesis and antimicrobial activity of quaternary ammonium-functionalized POSS (Q-POSS) and polysiloxane coatings containing Q-POSS. *Polymer* **2009**, *50*, 1124−1133.
(37) Sierke, J. K.; Ellis, A. V. High purity synthesis of a polyhedral oligomeric silsesquioxane modified with an antibacterial. *Inorg. Chem. Commun.* **2015**, *60*, 41−43.
(38) Chen, J.; Shan, J.; Xu, Y.; Su, P.; Tong, L.; Yuwen, L.; Weng, L.; Bao, B.; Wang, L. Polyhedral Oligomeric Silsesquioxane (POSS)-Based Cationic Conjugated Oligoelectrolyte/Porphyrin for Efficient Energy Transfer and Multiamplified Antimicrobial Activity. *ACS Appl. Mater. Interfaces* **2018**, *10*, 34455−34463.
(39) Tan, J.; Zhao, Y.; Hedrick, J. L.; Yang, Y. Y. Effects of Hydrophobicity on Antimicrobial Activity, Selectivity, and Functional Mechanism of Guanidinium-Functionalized Polymers. *Adv. Healthcare Mater.* **2022**, *11*, No. e2100482.
(40) Guo, W.; Wang, Y.; Wan, P.; Wang, H.; Chen, L.; Zhang, S.; Xiao, C.; Chen, X. Cationic amphiphilic dendrons with effective antibacterial performance. *J. Mater. Chem. B* **2022**, *10*, 456−467.
(41) Liu, Z.; Liu, Y. Multicharged cyclodextrin supramolecular assemblies. *Chem. Soc. Rev.* **2022**, *51*, 4786−4827.
(42) Bai, H.; Yuan, H.; Nie, C.; Wang, B.; Lv, F.; Liu, L.; Wang, S. A Supramolecular Antibiotic Switch for Antibacterial Regulation. *Angew. Chem., Int. Ed.* **2015**, *54*, 13208−13213.
(43) Yarlagadda, V.; Akkapeddi, P.; Manjunath, G. B.; Haldar, J. Membrane Active Vancomycin Analogues: A Strategy to Combat Bacterial Resistance. *J. Med. Chem.* **2014**, *57*, 4558−4568.
(44) Hughes, R. C.; Thurman, P. F.; Stokes, E. Estimates of the porosity of Bacillus licheniformis and Bacillus subtilis cell walls. *Z. Immunitatsforsch. Exp. Klin. Immunol.* **1975**, *149*, 126−135.
(45) Demchick, P.; Koch, A. L. The permeability of the wall fabric of *Escherichia coli* and Bacillus subtilis. *J. Bacteriol.* **1996**, *178*, 768−773.
(46) Chan, S.; Pullerits, K.; Keucken, A.; Persson, K. M.; Paul, C. J.; Rådström, P. Bacterial release from pipe biofilm in a full-scale drinking water distribution system. *NPJ Biofilms Microbiomes* **2019**, *5*, No. 9.
(47) Li, Y.; Fukushima, K.; Coady, D. J.; Engler, A. C.; Liu, S.; Huang, Y.; Cho, J. S.; Guo, Y.; Miller, L. S.; Tan, J. P. K.; Ee, P. L. R.; Fan, W.; Yang, Y. Y.; Hedrick, J. L. Broad-Spectrum Antimicrobial and Biofilm-Disrupting Hydrogels: Stereocomplex-Driven Supramolecular Assemblies. *Angew. Chem., Int. Ed.* **2013**, *52*, 674−678.
(48) Loddo, B.; Ferrari, W.; Brotzu, G.; Spanedda, A. In vitro Inhibition of Infectivity of Polio Viruses by Guanidine. *Nature* **1962**, *193*, 97−98.
(49) Gorbalenya, A. E.; Baker, S. C.; Baric, R. S.; de Groot, R. J.; Drosten, C.; Gulyaeva, A. A.; Haagmans, B. L.; Lauber, C.; Leontovich, A. M.; Neuman, B. W.; Penzar, D.; Perlman, S.; Poon, L. L. M.; Samborskiy, D. V.; Sidorov, I. A.; Sola, I.; Ziebuhr, J. The species Severe acute respiratory syndrome-related coronavirus: classifying 2019-nCoV and naming it SARS-CoV-2. *Nat. Microbiol.* **2020**, *5*, 536−544.
(50) Leong, J.; Shi, D.; Tan, J. P. K.; Yang, C.; Yang, S.; Wang, Y.; Ngow, Y. S.; Kng, J.; Balakrishnan, N.; Peng, S. Q.; Yeow, C. S.; Periaswamy, B.; Venkataraman, S.; Kwa, A. L.-H.; Liu, X.; Yao, H.; Yang, Y. Y. Potent Antiviral and Antimicrobial Polymers as Safe and Effective Disinfectants for the Prevention of Infections. *Adv. Healthcare Mater.* **2022**, *11*, No. e2101898.
(51) Kuroki, A.; Tay, J.; Lee, G. H.; Yang, Y. Y. Broad-Spectrum Antiviral Peptides and Polymers. *Adv. Healthcare Mater.* **2021**, *10*, No. 2101113.
(52) Bárcena, M.; Oostergetel, G. T.; Bartelink, W.; Faas, F. G. A.; Verkleij, A.; Rottier, P. J. M.; Koster, A. J.; Bosch, B. J. Cryo-electron tomography of mouse hepatitis virus: Insights into the structure of the coronavirion. *Proc. Natl. Acad. Sci. U.S.A.* **2009**, *106*, 582.
(53) Chin, W.; Yang, C.; Ng, V. W. L.; Huang, Y.; Cheng, J.; Tong, Y. W.; Coady, D. J.; Fan, W.; Hedrick, J. L.; Yang, Y. Y. Biodegradable Broad-Spectrum Antimicrobial Polycarbonates: Investigating the Role of Chemical Structure on Activity and Selectivity. *Macromolecules* **2013**, *46*, 8797−8807.

https://doi.org/10.1021/acsami.2c16493
ACS Appl. Mater. Interfaces 2023, 15, 354−363